Journal of Colloid and Interface Science 550 (2019) 57–63

Contents lists available at ScienceDirect

Journal of Colloid and Interface Science

journal homepage: www.elsevier.com/locate/jcis

Regular Article

Kinetics of sol-to-gel transition in irreversible particulate systems

Pai Liu [a,1], William R. Heinson [a,1,2], Christopher M. Sorensen [b], Rajan K. Chakrabarty [a,c,*]

[a] Center for Aerosol Science and Engineering, Department of Energy, Environmental and Chemical Engineering, Washington University in St. Louis, St. Louis, MO 63130, USA
[b] Department of Physics, Kansas State University, Manhattan, KS 66506, USA
[c] McDonnell Center for the Space Sciences, Washington University in St. Louis, St. Louis, MO 63130, USA

GRAPHICAL ABSTRACT

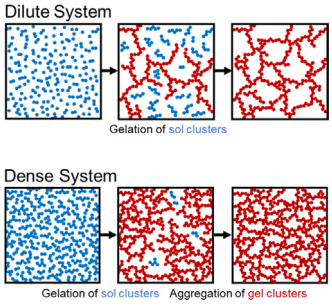

ARTICLE INFO

Article history:
Received 4 February 2019
Revised 21 April 2019
Accepted 22 April 2019
Available online 23 April 2019

Keywords:
Diffusion-limited cluster-cluster aggregation
Sol-to-gel transition
Percolation
Kinetics
Scaling laws
Characteristic timescales

ABSTRACT

A comprehensive theory encompassing the kinetics of the sol-to-gel transition is yet to be formulated due to break-down of the mean-field Smoluchowski Equation. Using high temporal-resolution Monte Carlo simulation of irreversible aggregation systems, we show that this transition has three distinct regimes with kinetic exponent $z \in [1, 2)$ corresponding to aggregation of sol clusters proceeding to the ideal gel point (IGP); $z \in [2, 5.7)$ for gelation of sol clusters beyond IGP; and $z \in [2, 3.5)$ for a hitherto unidentified regime involving aggregation of gels when monomer-dense. We further establish universal power-law scaling relationships that connect the kinetics of these three regimes. Improved parameterizations are performed on the characteristic timescale parameters that define each regime.

1. Introduction

Aggregation is a phenomenon ubiquitous in colloidal and aerosol systems [1–5]. Upon dispersion, particles collide and often irreversibly stick together to form larger clusters. Provided the monomer-monomer contact is non-coalescent, the aggregates manifest a scale-invariant, fractal-like morphology quantifiable with a mass fractal dimension (D_f) [1–3,6]. Prolonged aggregation leads to the phenomenon of gelation – a process involving the jamming together of ramified aggregates and the formation of volume-spanning networks with a characteristic $D_f \approx 2.5$ [7–11]. Gelation, as a phenomenon, has opened many avenues for synthesis of materials with unique properties [5,12–14]. The contemporary application of gelation theory extends to a broader context, for example, predicting the influence of wild fire emissions on climate change [15–17] and counteracting the formation of online extremist group

* Corresponding author at: Center for Aerosol Science and Engineering, Department of Energy, Environmental and Chemical Engineering, Washington University in St. Louis, St. Louis, MO 63130, USA.
E-mail address: chakrabarty@wustl.edu (R.K. Chakrabarty).
[1] These authors contributed equally to this work.
[2] Current addresses: Goddard Space Flight Center, National Aeronautics and Space Administration, Greenbelt, MD 20771, USA, and Earth Systems Science Interdisciplinary Center, University of Maryland, College Park, MD 20740, USA.

https://doi.org/10.1016/j.jcis.2019.04.067
0021-9797/

supports [18]. Despite its wide-ranging applicability, the theory of gelation still grapples with the fundamental questions "*How fast does a sol system gel and what are the associated critical time scales?*" The difficulty in formulating a comprehensive kinetic theory stems from the break-down, at the onset of gelation, of the mean-field assumption which lies at the core of the governing Smoluchowski Equation (SE) [6,8–10,19–21]. That is, SE, which tracks the time evolution of the system can only go so far in predicting the pre-onset of gelation, but not gelation itself [8,9]. An alternate successful interpretation of the sol-gel phenomenon is the percolation theory, which is a static model and hence, cannot predict the kinetics [22–24]. In this study, we address this long-standing problem by establishing a set of system-independent kinetic expressions capable of predicting the complete evolution of the sol-to-gel process. We do so by performing high temporal-resolution analysis on the evolution of diffusion limited cluster-cluster aggregation (DLCA) systems, which have been recently shown to produce gels that share identical morphologies with those produced via the percolation model [25].

This paper is organized as such: In Sections 1.1 and 1.2, we briefly revisit the traditional interpretations of the gelation tendency and kinetics, respectively. Concepts regarding the critical conditions that define the transition regimes are introduced. In Section 2, we describe the numerical methods used in simulating the irreversible DLCA process. In Section 3, we present the main results of this study, along with discussion on the time-evolution of cluster mass distribution, the power-law scaling relationships of the transition kinetics, and important characteristic timescales. We conclude this paper with Section 4.

1.1. Tendency of sol-to-gel transition

The tendency of gelation stems from the simple fact that the D_f of non-coalescent aggregates is always smaller than the spatial dimension (for example, $d = 3$ in three-dimensional space) [8,9]. As a result, when aggregates grow with $D_f < d$, the increase in their average size outruns their average nearest-neighbor separation. That said, the system inevitably evolves to crowded states [8,9]. When the total effective volume of all sol clusters reaches the system volume (V), the system is said to reach ideal gel point (IGP) [8,12]. Note that the effective cluster volume here is the perimeter volume (V_p), which could be visualized as volume of an isotropic sphere caging the cluster [26]. One should not be confused with the solid volume (V_m) of the cluster, which is the sum of the volumes of its constituent monomers. Visually, the IGP is the point at which sol clusters start to interdigitate [8,12], and it precedes the physical occurrence of the first gel cluster that spans the entire system volume. The point corresponding to the occurrence of such system-spanning gel is called physical gel point (PGP) or percolation point [8].

Past research has also outlined other methods to identify the onset of gelation in aggregation systems. For example, the occurrence of gel can be experimentally determined by observing the appearance of non-zero elasticity [21,27,28]. Theoretically, 1% of effective cluster volume fraction has also been shown as an indicator of imminent gelation [29], consistent with the onset of the cluster-dense regime [9], beyond which the aggregation system deviates from the SE dynamics.

1.2. Kinetics of sol-to-gel transition

The existing kinetic theory discusses the sol-to-gel transition within two major regimes [8–10,30]. Prior to IGP (hereafter Regime I), the transition is driven by the random collision and aggregation of particles that freely diffuse in system space, and the mean-field assumption holds valid [8–10,30]; Beyond the IGP (hereafter Regime II), the free space in the system is largely taken, and as a result, the motion of clusters is significantly restricted. From this point on, the interconnection among neighboring sol clusters starts to form, eventually leading to the onset of the gelling network [8–10,30]. When all aggregates in the system are incorporated into one single volume-spanning particle, the system is said to reach final gel state (FGS) [8].

The transition kinetics in Regime I is governed by the SE parameterized with aggregation kernels which depend on factors such as the relative motion between colliding particles and the cluster internal structure [6,8,19]. Solution to SE with homogeneous kernel leads to the scaling relationship between total number of clusters in the system (n_{tot}) and inverse time (t^{-1}), $n_{tot} \propto t^{-z}$, where the kinetic exponent (z) quantitatively measures how fast aggregation proceeds [8,9,26]. Regime I is further divided into two sub-regimes – cluster-dilute and dense – per the value of z [8]: Cluster-dilute regime describes the initial aggregation stage, during which Brownian kernel holds, yielding $z = 1$ [8,9,26]. Subsequently, the kinetics of aggregation tend to speed up as the system evolves to the cluster-dense regime, along with an increase in the value of z to about two near IGP [8,9]. A past theoretical modeling study found that the mean-field kinetics still holds valid although the kinetics is enhanced due to system crowding [9]. This finding is in good agreement with later experiments conducted on a reaction-limited system, wherein the second order kinetics is observed to prevail, even in extremely dense system very close to the gel point [21]. The kinetic modeling in Regime II remains an active research direction. Fry et al. empirically mapped the values of increasing z with respect to t for the DLCA systems transitioning between IGP and FGS (i.e. the Post-IGP Regime) [9]. Rottereau et al. quantitated the late-stage process using the concepts as evolution of connectivity between clusters [10]. However, no explicit kinetic expression has been formulated for Regime II to our knowledge. Purely mathematical based analysis – an application of SE while disregarding the breaking down of mean-field assumption – has led to the advent of mathematical gelation [31]. Such a model, however, has been shown to ultimately fail on real world colloidal systems [30]. Lushnikov introduced a truncated model by immediately removing heavy particles (gels) with mass greater than a cutoff value, which reconciles the paradoxical behavior of SE, at a cost of violating mass conservation [32].

2. Methods

Our off-lattice DLCA model follows that introduced in previous publications [33,34]. The model algorithm starts out by generating a cubic simulation box with three-million randomly placed monomers. The monomer volume fraction (f_{vm}) is controlled by specifying the V of the simulation box,

$$f_{vm} = \frac{4}{3}\pi a^3 \frac{n_{tot,0}}{V} \tag{1}$$

where a is a monomer radius in arbitrary units, and $n_{tot,0}$ denotes the total number of particle (cluster) at $t = 0$, which is equal to the conserved total number of monomers in the system. The simulation proceeds by randomly picking a cluster of mass N (number of constituent monomers, and $N = 1$ for monomer) and moving it by $2a$ in a random direction with probability N^{-1/D_f} per Stokes-Einstein diffusion [19]. The algorithm tracks the total number of clusters (n_{tot}), and once every n_{tot} clusters have been picked, t is incremented by unit simulation time t_s. We define t_s as the time-interval during which monomers move by a root-mean-squared-displacement of $2a$ (See Supplementary Sect. I for derivation):

$$t_s = \frac{4\pi\mu a^3}{k_B T} \tag{2}$$

where k_B, T, and μ respectively represent the Boltzmann constant, temperature, and viscosity of the surrounding gas [19]. During the process, if two clusters collide, they are joined together forming a new cluster, and n_{tot} decreases by one. The above procedure was repeated until $n_{tot} = 1$, that is, the FGS was attained, and the corresponding time t_{FGS} was recorded. By the end of each run, the algorithm outputted a list for cluster N for every t which incremented by t_s in the range between 0 and t_{FGS}. We next calculated, from the list, the cluster mass frequency distribution (hereafter, mass distribution), written as $n(\log_{10}N, t/t_s)/n_{tot}(t/t_s)$ where n denotes the number of clusters having N monomers at time t.

3. Results and discussion

3.1. Evolution of cluster mass distribution

Fig. 1 shows the contour plots of aggregate mass distributions in the $\log_{10}N - t/t_s$ space for systems of various f_{vm}. Panel (a) demonstrates the mean-field growth of sol clusters which is typically seen in Regime I, during which the kinetics could be described with the exact solution to SE [8,9,19,26].

Next, we discuss the onset of gelation and the subsequent Regime II by comparing the cluster mass distributions with the analytical solution values of average cluster mass at the IGP (written as N_{IGP}):

$$N_{IGP} = k_0 \left(R_{g,IGP}/a\right)^{D_f} \tag{3.1}$$

$$\text{with } R_{g,IGP} = a\left[f_{vm}^{-1} k_0 \left(\frac{D_f}{D_f+2}\right)^{3/2}\right]^{1/\left(3-D_f\right)} \tag{3.2}$$

where $R_{g,IGP}$ is the average radius of gyration (a linear size) of aggregates at the IGP and k_0 is the fractal prefactor in the scaling relation. Eq. (3.1) follows mass scaling power-law relationship with $k_0 = 1.3$ and $D_f = 1.8$ describing the morphology of DLCA. Eq. (3.2), originally introduced in Ref. [35], is reached when one equalizes the system V to the total cluster V_P.

Panel (b)–(e) show that when sol clusters grow, their geometric mean mass value, represented by $\langle \log_{10}N \rangle$ (red dashed lines), asymptotes to the $\log_{10}N_{IGP}$ value (red solid lines) predicted by Eq. (3). Subsequently, the IGP could be identified at the point when $\langle \log_{10}N \rangle$ reaches $\log_{10}N_{IGP}$ (See Supplementary Sect. II), and the corresponding time is regarded as the ideal gel time (t_{IGP}). In Fig. 1 we mark the IGP at the points $(N = N_{IGP}, t = t_{IGP})$ using triangle symbols. One could observe that immediately after IGP, the mass distribution (in Fig. 1(b)–(e)) becomes bimodal, indicating the onset of a separate phase, the gel. Subsequently, the gel clusters in the systems continuously grow by scavenging the remaining sol clusters whose mass distribution stays invariant with $\langle \log_{10}N \rangle$ closely matching $\log_{10}N_{IGP}$. In the dilute systems with $f_{vm} = 0.005$, 0.01, and 0.02, the gel clusters grow in a rapid manner and the biggest gel reach a mass of about 10^6 at $t/t_{IGP} \approx 1.5$, 1.7, and 2.3, respectively. One could infer the onset of the system spanning gel (the PGP) when the mass of the biggest gel cluster reaches the order-of-magnitude of $n_{tot,0}$. In the denser system with $f_{vm} = 0.05$ and 0.1, counter-intuitively, the mass of the biggest gel cluster reaches $\sim 10^6$ at much later times, $t/t_{IGP} \approx 10.2$ and 28.8, respectively, which are very close to the FGS ($N = n_{tot,0}, t = t_{FGS}$, circle symbols in Fig. 1). This observation implies that gel clusters in the denser systems tend to form in a local manner. Those freshly produced gel clusters percolate a sub-volume of the system, instead of the entire system. The system-spanning gel is formed near the very end of the transition, when the all local gel clusters are assembled together.

Another important observation from the evolution of mass-distribution is that beyond IGP, a considerable amount of time is

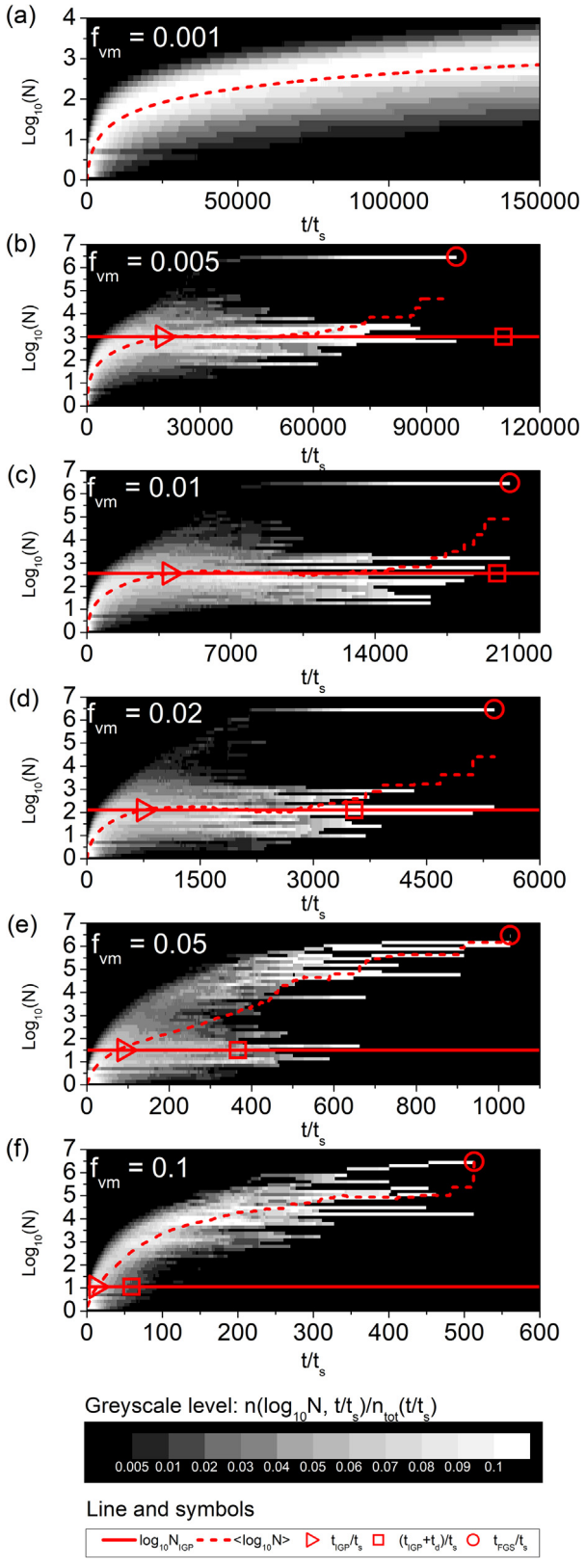

Fig. 1. Time-evolution of the aggregate mass distribution for DLCA systems with $f_{vm} = 0.001$ (a), 0.005 (b), 0.01 (c), 0.02 (d), 0.05 (e), and 0.1 (f). The solid lines represent the analytical solution values to the characteristic cluster mass at the IGP, $\log_{10}N_{IGP}$, which follows Eq. (3). The dashed lines represent the geometric mean values of cluster mass, $\langle \log_{10}N \rangle$. In panels (b)–(f), triangles and circles, respectively, represent t_{IGP} and t_{FGS}, which are determined from the simulations. Squares indicate the time when sol clusters deplete, $t_{IGP} + t_d$, and t_d is solved using Eq. (4). All timescales are presented in units of t_s.

always needed for the total conversion of sol clusters to gel phase, as shown in Fig. 1. We next discuss how to quantify the length of the time interval between IGP and the total conversion of sol clusters, which is written as t_d in the context of this paper. Recall that IGP is the point where the perimeter volume fraction of sol clusters reaches unity [8,35]. Such a condition, however, does not guarantee the immediate formation of the interconnection among neighboring sol clusters (hence t_d exists). This seemingly contradictory observation can be explained by the fact that fractal clusters only partially fill the Euclidean space. In other words, free spaces within the V_p always exist, so that the neighboring sol clusters at IGP could remain interdigitating, instead of forming connections (such configuration is qualitatively described by the schematic diagram in Fig. 2). Quantitatively, we measure the free spaces with $V_{p,IGP} - V_{m,IGP}$ (subscripts indicating parameters at IGP). This volume difference, when raised to power of 2/3, yields a square of a length scale whose square root approximately measures the average distance by which clusters need to travel in order to connect with their neighbors. Write the diffusivity of cluster at IGP as D_{IGP}, and the rearrangement of diffusion equation in three dimensional space yields to $t_d = \frac{\left(V_{p,IGP}-V_{m,IGP}\right)^{2/3}}{6D_{IGP}}$. We show a step-by-step derivation in Supplementary Sect. III that t_d, after being normalized by t_s, is a function of f_{vm} only, written as:

$$\frac{t_d}{t_s} = \frac{1}{4}\left[\frac{4}{3}\pi(1-f_{vm})\right]^{2/3}\left(\frac{D_f}{D_f+2}\right)^{(2D_f+3)/(6-2D_f)}\left(k_0 f_{vm}^{-1}\right)^{3/(3-D_f)} \quad (4)$$

In Fig. 1 we mark the critical points corresponding to the total conversion of sol clusters at $(N = N_{IGP}, t = t_{IGP} + t_d)$ using square symbols. Good agreements between the predictions by Eq. (4) and the simulations are seen for systems with different f_{vm}. Another important inference from our scaling analysis is that t_d is inversely related to the f_{vm}. Qualitatively, this is because a denser system (with higher f_{vm}) reaches IGP with average sol clusters of smaller N_{IGP}, which are in turn characterized with smaller $V_{p,IGP} - V_{m,IGP}$, and simultaneously larger D_{IGP}. One could also observe such inverse correlation between t_d and f_{vm} in Fig. 1(b)–(e). For example, when a system is sufficiently dilute ($f_{vm} = 0.005$ and 0.01), the total conversion of sol clusters occurs at a timescale comparable to that of the FGS, formally $t_{IGP} + t_d \approx t_{FGS}$. With a further increase in f_{vm} (from 0.02 to 0.05), t_d decreases, the total conversion of sol clusters precedes FGS, and the time interval between $t_{IGP} + t_d$ and t_{FGS} becomes non-trivial. Such tendency reaches an extremity when $f_{vm} = 0.1$, as shown in Fig. 1(f), where $t_{IGP} + t_d \ll t_{FGS}$ and the system evolves with a unimodal cluster mass distribution throughout the entire process. This unimodality implies that sol clusters and gels no longer coexist. For these extremely dense systems ($f_{vm} = 0.05$ and 0.1), the transition process beyond the $t_{IGP} + t_d$ is defined as Regime III, which differs fundamentally from the classical picture of sol-to-gel transition [8].

3.2. Scaling law for aggregation and gelation kinetics

We next demonstrate that the kinetics within Regimes I, II and III could be unified on coherent power-law relationships, when the transition is observed with two timescales, first, the characteristic time for Brownian aggregation (t_c), and second, the t_{IGP}. In Regime I, solving SE with homogeneous Brownian kernel provides the scaling law with $z = 1$ [8,19]:

$$\frac{n_{tot}}{n_{tot,0}} = \left(1 + \frac{t}{t_c}\right)^{-1} \quad (5)$$

$$\text{and, } t_c = \frac{3\mu V}{4k_B T n_{tot,0}} \quad (6)$$

According to Eq. (5) we empirically determine t_c from DLCA simulations at the time when n_{tot} decreases to half of the initial values (See Supplementary Sect. IV).

Fig. 3(a) shows that when t is normalized per $1 + t/t_c$, the early stages of the transition are unified and the trends of $n_{tot}/n_{tot,0}$ follow Eq. (5) with $z = 1$, indicating the dominance of Brownian aggregation mechanism. This is especially true for $f_{vm} = 0.001$, whereas the behavior becomes more rapid than Eq. (5) for progressively larger f_{vm}. This deviation from Eq. (5) indicates subsequent cluster-dense conditions, and the kinetics speed up with the kinetic exponent z taking on values larger than unity, during which the driving mechanism of aggregation becomes ballistic-limited as the interdigitating aggregates have no more free space to diffuse [8,9,36].

Fig. 3(b) shows the late-stages of the transition are unified upon normalizing t according to $1 + t/t_{IGP}$. A universal power-law relationship manifests as,

$$\frac{n_{tot}}{n_{tot,IGP}} = 2^{z_{FGS}}\left(1 + \frac{t}{t_{IGP}}\right)^{-z_{FGS}} \quad (7)$$

where $z_{FGS} \approx 5.7$ is the kinetic exponent reported at the FGS [9]. The z takes on a terminal value because only when $t \gg t_{IGP}$ (that is, FGS) could Eq. (7) be reduced to $n_{tot} \propto t^{-z}$. The prefactor takes up the expression of $2^{z_{FGS}}$, satisfying $n_{tot} = n_{tot,IGP}$ when $t = t_{IGP}$. The two power-law relationships, Eq. (5) and the new Eq. (7) provide a complete description for the full so-to-gel transition within regimes I and II.

Regime III occurs in system $f_{vm} = 0.1$ with a counterintuitively slower kinetics. Fig. 3(c) shows that the decrease in $n_{tot}/n_{tot,0}$ for $f_{vm} = 0.1$ falls behind that for $f_{vm} = 0.05$. When observed with $1 + t/t_{IGP}$, a less steep decreasing trend of $n_{tot}/n_{tot,IGP}$ is seen (Panel (d)) when $f_{vm} = 0.1$. Eq. (7) still holds valid while a $z_{FGS} \approx 3.5$ fits the data best, per the red solid line in panel (d). This slower rate – in a denser system – could be due to the abundance gel clusters which are considerably less mobile. Qualitatively speaking, the extremely dense system facilitates almost an instantaneous gelation of sol clusters, but the resultant abundance of gels slows down the system progressing from IGP to FGS. Fig. 3(d) shows that the decreasing trend of $n_{tot}/n_{tot,IGP}$ for the system with $f_{vm} = 0.05$ originally follows Eq. (7) with $z_{FGS} \approx 5.7$ until reaching an inflection point indicated by the arrow in (d). Beyond the inflection, the trend asymptotes to the less steep one governed by $z_{FGS} \approx 3.5$. Note that this inflection occurs approximately at $t_{IGP} + t_d$ of the system (see Fig. 1(e)), indicating that a slowing down of kinetics is indeed a characteristic of the system in which only gel clusters exist. These dense gelation systems near $f_{vm} = 0.1$ are traditionally discussed in the frame work of static percolation and thermodynamics [22–25] and here we emphasize that the kinetic aspect should not be overlooked.

3.3. Improved parameterization on characteristic timescales

We next evaluate the existing analytical expressions for the important characteristic timescales that are involved in the sol-to-gel transition process. Combining Eq. (6) with (1) and (2) yields the analytical expression for t_c in units of t_s:

$$\frac{t_c}{t_s} = \frac{1}{4} f_{vm}^{-1} \quad (8)$$

Fig. 4 compares the prediction of Eq. (8) with the t_c/t_s determined from simulations. The exponent -1 fails at large f_{vm}, indicating that the aggregation in these extremely dense systems deviates from the Brownian kernel at a very early point. The enhanced kinetics lead to the t_c being smaller than what Eq. (8) predicts. The upper limit for f_{vm} is the percolation threshold, at

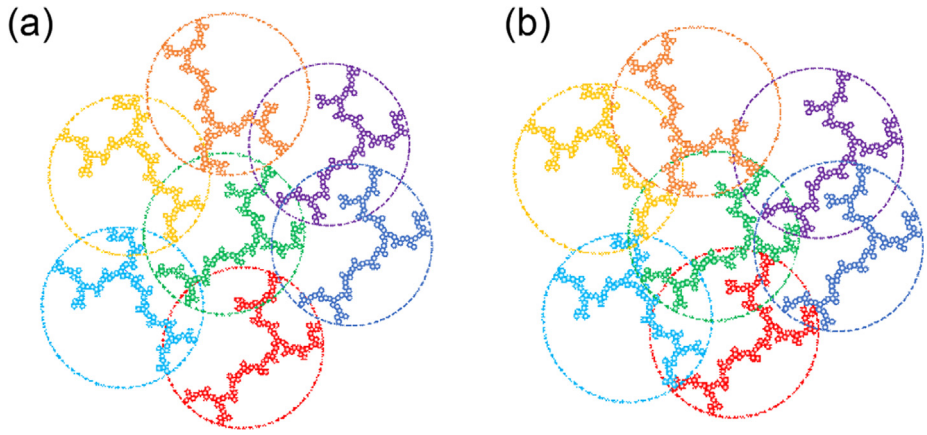

Fig. 2. Schematic diagrams showing the interdigitating (a) and connected (b) fractal clusters. Individual clusters are colored differently. Dashed circle represents the effective volume of the clusters. In (a), fractal clusters highly interdigitate. Although the effective volume of clusters saturates the system, connections among clusters are not guaranteed. In this case, clusters could still move around freely until they connect with their neighbors. (b) shows the condition at which all clusters are connected, resulting in the onset of gel.

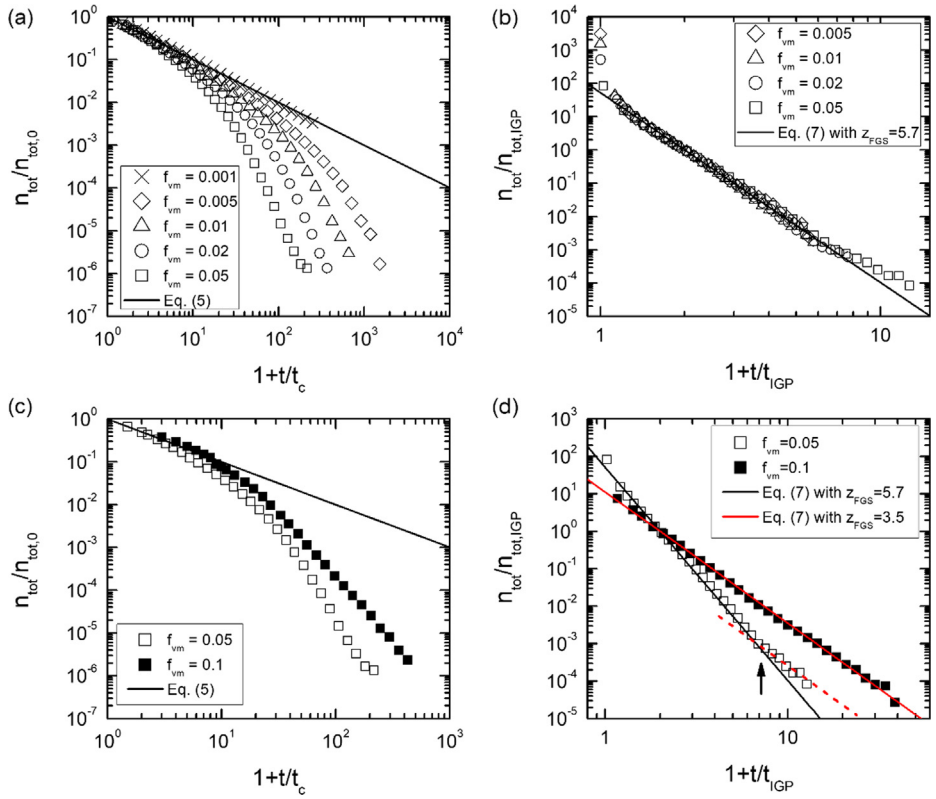

Fig. 3. (a) and (c) show that early stages of aggregation are unified by Eq. (5) when observed with normalized time $1 + t/t_c$. (b) and (d) show that the late stages of transitions, when observed with normalized time $1 + t/t_{IGP}$, are unified by Eq. (7). Dashed line in (d) has a slope of −3.5, and the arrow indicates an inflection in transition kinetics.

which point the volume-spanning gel is instantaneously formed, and so that both t_c and t_{IGP} decrease to zero. Ref [37] reports the critical volume fraction (Φ_P) to be about 0.18 (black line in Fig. 4) at which a system of randomly packed hard spheres reaches percolation threshold in three-dimensional space. We introduce a semi-empirical expression of t_c for the dense DLCA systems near the percolation threshold as

$$\frac{t_c}{t_s} = \frac{1}{4}\left(f_{vm}^{-1} - \Phi_P^{-1}\right) \tag{9}$$

The prediction by Eq. (9) is plotted in Fig. 4 and it captures the dramatic decrease in the t_c/t_s near Φ_P. Similarly, we provide an improved parameterization of t_{IGP} for these dense DLCA systems,

$$\frac{t_{IGP}}{t_s} = \frac{1}{4}\left(f_{vm}^{-1} - \Phi_P^{-1}\right)\left[b^{-\frac{1}{z}} f_{vm}^{\frac{D_f}{(D_f-3)z}}\left(\frac{D_f}{D_f+2}\right)^{\frac{3D_f}{(6-2D_f)z}} k_0^{\frac{3}{(3-D_f)z}} - 1\right] \tag{10}$$

where b originates from a power-law relationship $\langle N\rangle = b(1 + t/t_c)^z$ quantifying the aggregate growth when cluster-dense condition sets in [26]. The step-by-step derivation of Eq. (10) is outlined in

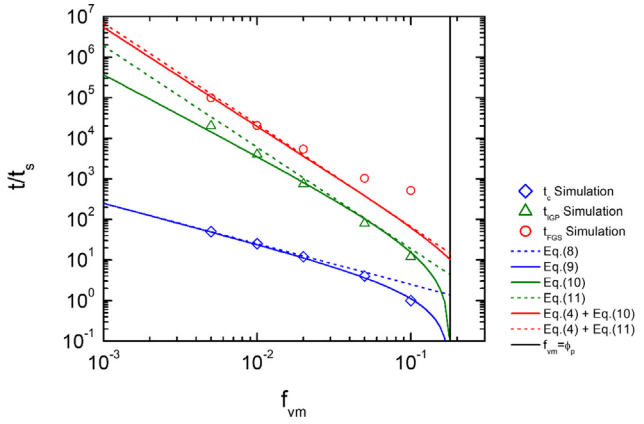

Fig. 4. Characteristic timescales t_c, t_{IGP} and t_{FGS} as functions of f_{vm}. The timescale parameters determined from DLCA simulations are compared with their analytical solution values.

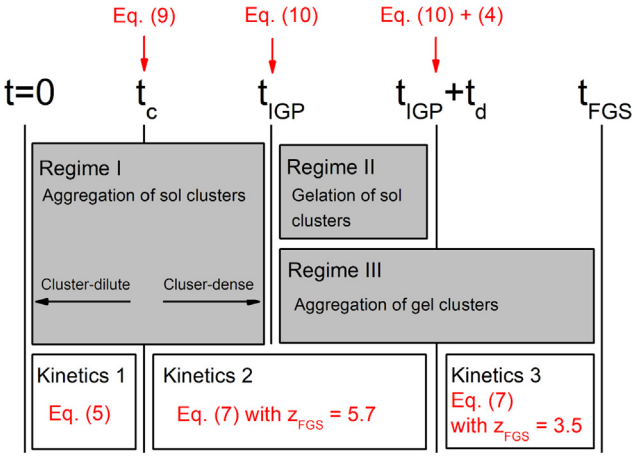

Fig. 5. The kinetics of full sol-to-gel transition.

Supplementary Sect. V. The determination of the values for b and z from DLCA is discussed in Sect. VI. Fig. 4 also compares the prediction of Eq. (10) (solved with $D_f = 1.8$, $k_0 = 1.3$, $z = 1.5$ and $b = 0.2$) to the t_{IGP}/t_s determined from simulations. The traditionally used expression [8,12] for t_{IGP} is also evaluated here: $t_{IGP} \approx a^3 K^{-1} f_{vm}^{-2.5}$, which after being combined with Eq. (2) yields to:

$$\frac{t_{IGP}}{t_s} = \frac{3}{16\pi} f_{vm}^{-2.5} \tag{11}$$

Fig. 4 shows that Eq. (11) overestimates t_{IGP} by a factor less than two.

The summation of Eq. (10) (or (11)) and (4) provide analytical solution values for $(t_{IGP} + t_d)/t_s$, which are compared with the t_{FGS}/t_s determined from simulations. We again observe that a dilute system reaches FGS when the total conversion of sol clusters is attained ($t_{IGP} + t_d \approx t_{FGS}$), but when monomer dense, the time interval between $t_{IGP} + t_d$ and t_{FGS} becomes significant, during which regime III takes over the kinetics. Fig. 4 and Eqs. (4), (8)–(11) also show that the timescale parameters – t_c, t_{IGP}, and t_d – are functions of f_{vm} only. Those parameters are scale-independent. Their values are not sensitive to changes in system size V, as long as f_{vm} is fixed. Note that the parameters, n_{tot} and t_{FGS}, however, are scale-dependent. Their values are sensitive to system size and hence they are functions of both f_{vm} and V. We show in Supplementary Sections VII that $n_{tot} \propto V$, and $t_{FGS} \propto V^{1/z_{FGS}}$. The dependence of t_{FGS} on V is rather insignificant when system is dilute, because z_{FGS} takes a value as large as 5.7. The influence of system scale becomes pronounced when system is dense. At last, we need to emphasize that the entire discussion of scale-independence is built upon an important prerequisite – that the system should be at least large enough, such that for any given f_{vm}, the $n_{tot,0}$ is always much larger than N_{IGP}. This condition guarantees that statistically significant amount of clusters exist in the system beyond IGP.

4. Conclusion

We conclude the paper with Fig. 5 which schematically illustrates the comprehensive picture. The transition Regimes I-III and the corresponding kinetic formulations (Eqs. (5) and (7)) are presented with the characteristic timescales, t_c, t_{IGP}, and $t_{IGP} + t_d$ serving as milestones. Please note that the regime I and II are separated per t_{IGP} at which point SE breaks down, but kinetics 1 fails at $t \approx t_c$ when Brownian aggregation kernel no longer holds valid (the cluster-dense condition sets in) [8,9]. Regime II and III start out simultaneously at IGP, but II tends to dominate over III because number of gel clusters in a system is typically negligible compared to that of the sol clusters. Regime III only takes precedence after II reaches its completion, that is $t_{IGP} + t_d < t < t_{FGS}$, which only manifests when monomer-dense. The latest study [38] on the gelation in DLCA system with $f_{vm} = 0.1$ reveals a breakdown of the invariance between the mass and surface fractal dimension values for monomer-dense gels. This observation indicates that Regime III is indeed a distinct transition process, with regard to both kinetics and the morphologies of resultant gel particles. Future research on this topic should be directed toward experimental studies on the late-stage Regime III in the dense aggregation systems, with an emphasis placed on the kinetic perspective. Another interesting topic for future research is to investigate the gelation kinetics in the systems with f_{vm} varying as a function of t. For example, changing system V as aggregation proceeds, which has been shown critical in studying more realistic aggregation systems with polydispersed constituent monomers [39].

Acknowledgements

This work has been supported by the US National Science Foundation (NSF) grants AGS-1455215, CBET-1511964, AGS-1649783 and AGS-1623808, and the NASA Radiation Sciences Program grant NNX15AI66G.

Appendix A. Supplementary material

Supplementary data to this article can be found online at https://doi.org/10.1016/j.jcis.2019.04.067.

References

[1] F. Hausdorff, Dimension und äußeres Maß, Math. Ann. 79 (1918) 157–179.
[2] S.R. Forrest, T.A. Witten Jr., Long-range correlations in smoke-particle aggregates, J. Phys. A 12 (1979) L109.
[3] C.M. Sorensen, The mobility of fractal aggregates: a review, Aerosol Sci. Technol. 45 (2011) 765–779.
[4] F. Family, D.P. Landau, Kinetics of Aggregation and Gelation, Elsevier, Massachusetts, USA, 1984.
[5] C.J. Brinker, G.W. Scherer, Sol-gel Science: the Physics and Chemistry of Sol-gel Processing, Academic Press, New York, USA, 2013.
[6] P. Sandkühler, J. Sefcik, M. Lattuada, H. Wu, M. Morbidelli, Modeling structure effects on aggregation kinetics in colloidal dispersions, AIChE J. 49 (2003) 1542–1555.
[7] C.M. Sorensen, W.B. Hageman, T.J. Rush, H. Huang, C. Oh, Aerogelation in a flame soot aerosol, Phys. Rev. Lett. 80 (1998) 1782.
[8] C.M. Sorensen, A. Chakrabarti, The sol to gel transition in irreversible particulate systems, Soft Matter 7 (2011) 2284–2296.

[9] D. Fry, T. Sintes, A. Chakrabarti, C.M. Sorensen, Enhanced kinetics and free-volume universality in dense aggregating systems, Phys. Rev. Lett. 89 (2002) 148301.
[10] M. Rottereau, C.J. Gimel, T. Nicolai, D. Durand, Monte Carlo simulation of particle aggregation and gelation: I. Growth, structure and size distribution of the clusters, Eur. Phys. J. E 15 (2004) 133–140.
[11] R. Dhaubhadel, F. Pierce, A. Chakrabarti, C.M. Sorensen, Hybrid superaggregate morphology as a result of aggregation in a cluster-dense aerosol, Phys. Rev. E 73 (2006) 011404.
[12] R. Dhaubhadel, C.S. Gerving, A. Chakrabarti, C.M. Sorensen, Aerosol Sci. Technol. 41 (2007) 804–810.
[13] R.K. Chakrabarty, I.V. Novosselov, N.D. Beres, H. Moosmüller, C.M. Sorensen, C. B. Stipe, Trapping and aerogelation of nanoparticles in negative gravity hydrocarbon flames, Appl. Phys. Lett. 104 (2014) 243103.
[14] P. Liu, I.J. Arnold, Y. Wang, Y. Yu, J. Fang, P. Biswas, R.K. Chakrabarty, Synthesis of titanium dioxide aerosol gels in a buoyancy-opposed flame reactor, Aerosol Sci. Technol. 49 (2015) 1232–1241.
[15] R.K. Chakrabarty, N.D. Beres, H. Moosmüller, S. China, C. Mazzoleni, et al., Soot superaggregates from flaming wildfires and their direct radiative forcing, Sci. Rep. 4 (2014) 5508.
[16] S.P. Kearney, F. Pierce, Evidence of soot superaggregates in a turbulent pool fire, Combust. Flame 159 (2012) 3191–3198.
[17] W.R. Heinson, R.K. Chakrabarty, Fractal morphology of black carbon aerosol enhances absorption in the thermal infrared wavelengths, Opt. Lett. 41 (2016) 808–811.
[18] P.D. Manrique, M. Zheng, Z. Cao, E.M. Restrepo, N.F. Johnson, Generalized gelation theory describes onset of online extremist support, Phys. Rev. Lett. 121 (2018) 048301.
[19] S.K. Friedlander, Smoke, Dust, and Haze: Fundamentals of Aerosol Dynamics, Oxford University Press, New York, USA, 2000.
[20] M. Lattuada, P. Sandkühler, H. Wu, J. Sefcik, M. Morbidelli, Aggregation kinetics of polymer colloids in reaction limited regime: experiments and simulations, Adv. Colloid Interface Sci. 103 (2003) 33–56.
[21] P. Sandkühler, J. Sefcik, M. Morbidelli, Kinetics of aggregation and gel formation in concentrated polystyrene colloids, J. Phys. Chem. B 108 (2004) 20105–20121.
[22] D. Stauffer, Gelation in concentrated critically branched polymer solutions. Percolation scaling theory of intramolecular bond cycles, J. Chem. Soc. Faraday Trans. 2 (72) (1976) 1354.
[23] P.G. DeGennes, On a relation between percolation theory and the elasticity of gels, J. Phys. Lett. Paris 37 (1976) 1–2.
[24] D. Stauffer, A. Coniglio, M. Adam, Gelation and critical phenomena, Adv. Polym. Sci. 44 (1982) 103.
[25] W.R. Heinson, A. Chakrabarti, C.M. Sorensen, Kinetic percolation, Phys. Rev. E 95 (2017) 052109.
[26] C. Oh, C.M. Sorensen, Light scattering study of fractal cluster aggregation near the free molecular regime, J. Aerosol Sci. 28 (1997) 937–957.
[27] A. Zaccone, H. Wu, E. Del Gado, Elasticity of arrested short-ranged attractive colloids: Homogeneous and heterogeneous glasses, Phys. Rev. Lett. 103 (2009) 208301.
[28] K. Kroy, M.E. Cates, W.C.K. Poon, Cluster mode-coupling approach to weak gelation in attractive colloids, Phys. Rev. Lett. 92 (2004) 148302.
[29] M.C. Heine, S.E. Pratsinis, Brownian coagulation at high concentration, Langmuir 23 (2007) 9882–9890.
[30] P. Sandkühler, J. Sefcik, M. Morbidelli, Kinetics of gel formation in dilute dispersions with strong attractive particle interactions, Adv. Colloid Interface Sci. 108 (2004) 133–143.
[31] P.G.J. Van Dongen, M.H. Ernst, Dynamic scaling in the kinetics of clustering, Phys. Rev. Lett. 54 (1985) 1396.
[32] A.A. Lushnikov, Gelation in coagulating systems, Physica D 222 (2006) 37–53.
[33] W.R. Heinson, P. Liu, R.K. Chakrabarty, Fractal scaling of coated soot aggregates, Aerosol Sci. Technol. 51 (2017) 12–19.
[34] P. Meakin, Computer simulation of cluster-cluster aggregation using linear trajectories: results from three-dimensional simulations and a comparison with aggregates formed using Brownian trajectories, J. Colloid Interface Sci. 102 (1984) 505–512.
[35] D. Fry, A. Chakrabarti, W. Kim, C.M. Sorensen, Structural crossover in dense irreversibly aggregating particulate systems, Phys. Rev. E 69 (2004) 061401.
[36] P. Liu, W.R. Heinson, B.J. Sumlin, K. Shen, R.K. Chakrabarty, Establishing the kinetics of ballistic-to-diffusive transition using directional statistics, Phys. Rev. E 97 (2018) 042102.
[37] M.J. Powell, Site percolation in randomly packed spheres, Phys. Rev. B 20 (1979) 4194.
[38] W.R. Heinson, Y.W. Heinson, P. Liu, R.K. Chakrabarty, Breakdown of fractal dimension invariance in high monomer-volume-fraction aerosol gels, Aerosol Sci. Technol. 52 (2018) 953–956.
[39] E. Goudeli, M.L. Eggersdorfer, S.E. Pratsinis, Coagulation of agglomerates consisting of polydisperse primary particles, Langmuir 32 (2016) 9276–9285.